VOL. 13, NO. 3 J. HYDRONAUTICS JULY 1979

ARTICLE NO. 78-265R

Measurements of Vertical Profiles of Oceanic Current and Richardson Number near St. Croix, U.S.V.I.

D. C. Wenstrand*
The Johns Hopkins University, Laurel, Md.

Measurements of vertical profiles of both horizontal components of ocean current were made approximately 6 kilometers from the western shore of St. Croix, U.S. Virgin Islands, with a vertical array of current meters, and using the technique of acoustically tracking slowly sinking floats. During some of the drops, the local profile of Väisälä frequency was measured by lowering a CTD (conductivity, temperature, depth) from a ship positioned directly over the descending profiler. Richardson numbers computed from these data were typicaly between 1 and 10, with values as small as 0.25 occurring occasionally. Simultaneous drops at different locations showed significant loss of similarity at separations of 2 km, and drops made at a fixed location became decorrelated in several hours.

Introduction

THE spectrum of internal waves in the ocean has been shown to be remarkably homogenous, as evidenced by the ability of Garrett and Munk[1,2] and Desaubies[3] to fit a universal spectral model to a diverse set of observations. This homogeneity of the oceanic internal wave field is suggestive of either a homogenous forcing mechanism or saturation of the wave field, or both. It has been pointed out by Wunsch[4] that it is the departures from homogeneous models that should be studied in order to gain an understanding of the mechanisms by which internal waves are generated and dissipated.

All of the measurements presented in this artical were made in proximity to the island of St. Croix and therefore might be expected to differ somewhat from similar observations made in the open ocean. Since it was not known how nearby topography would affect the distribution of internal wave energy with respect to frequency and vector wave number, several types of measurements were performed. To characterize the vertical current structure, 58 current profiler drops were made to a maximum depth of 400 m. Drops were made at a fixed location every 1 to 4 h to assess temporal variability of the profile, and simultaneous, spatially separated drops were made with two profilers to determine spatial variability. Also, an array of vector-averaging current meters was deployed to supplement the current profile measurements.

The data presented here are only a fraction of those available, and were chosen to show the kind of information that was obtained and to illustrate some of the more salient features of the current structure and variability that were observed.

Instrumentation and Experimental Technique

The technique of acoustically tracking slowly sinking floats to measure current profiles has been used by several investigators. Most measurements, such as those by Rossby,[5] have employed existing tracking facilities, though some, namely those of Pochapsky,[6] have utilized portable tracking equipment. The measurements reported on herein were all performed on the AFWR St. Croix Underwater Range, which is operated for the U. S. Navy by RCA.

The circles in Fig. 1 show the tracking coverage provided by each of the 11 underwater arrays of hydrophones. Each array consists of four hydrophones† located at the adjacent vertices of a cube with 9.1 m side length (Fig. 2). An object being tracked emits a timed 75-kHz pulse every 1.31072 s. The times of arrival of this pulse at each hydrophone, together with the known time when it was emitted, are then used to compute the object's position relative to array center. The coordinates of the object relative to the center of the cube are

$$x_i = (V_s^2/2d)(t_c^2 - t_i^2) \qquad i = 1,2,3 \qquad (1)$$

where V_s is the speed of sound, d is the cube side length, and where t_c and t_i are pulse transit times to the corner and x_i hydrophones, respectively. This formula must be corrected for refraction or ray-bending resulting from the approximately 3% variation in sound-speed over the 1000-m water column. This correction, along with several others which were applied to the tracking data as part of the standard range processing, is discussed in detail by Sandstrom.[7] To minimize errors in the ray-bending corrections that could result from uncertainties in the sound velocity profile, most drops were made within 500 m of the array center. (This also reduced the point-to-point noise in the tracking data.)

As can be seen from Eq. (1), the accuracy of the position determination rests on the accuracy to which the transit times t_c and t_i are known. By taking the differential of Eq. (1), we obtain a relation between the uncertainty in x_i and the uncertainties in the transit times Δt_c and Δt_i:

$$\Delta x_i = (V_s^2/d)(t_c \Delta t_c - t_i \Delta t_i) \qquad (2)$$

Assuming that the timing errors are independent random variables with the same variance and zero mean gives

$$\langle \Delta x_i^2 \rangle = (V_s^4/d^2)(t_c^2 + t_i^2)\langle \Delta t^2 \rangle \qquad (3)$$

Since the array dimension d is nearly always small compared to the slant range R to the object being tracked, Eq. (3) becomes

$$\langle \Delta x_i^2 \rangle^{1/2} = \frac{\sqrt{2} R V_s}{d} \langle \Delta t^2 \rangle^{1/2} \qquad (4)$$

Presented as Paper 78-265 at the AIAA 16th Aerospace Sciences Meeting, Huntsville, Ala., Jan. 16-18, 1978; submitted July 7, 1978; revision received March 14, 1979.

Index categories: Marine Instrumentation; Oceanography, Physical and Biological.

*Physicist, Applied Physics Laboratory. Member AIAA.

†Actually some arrays contain a redundant fifth hydrophone, which is operated if one of the primary hydrophones malfunctions.

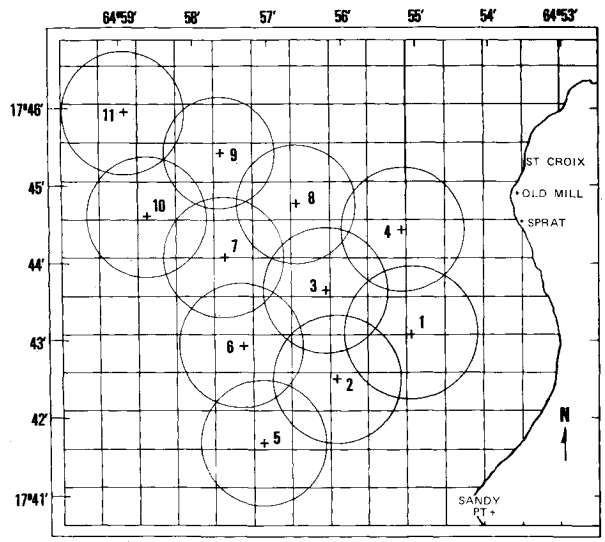

Fig. 1 AFWR St. Croix Underwater Range. Circles indicate approximate coverage of the 11 underwater arrays of hydrophones that were present when the present measurements were made. In November 1976, two new arrays were added, and the existing arrays were renumbered.

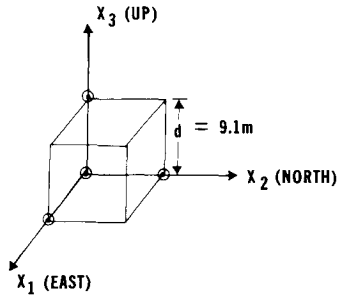

Fig. 2 Schematic of tracking array geometry. Hydrophones are located at the circled corners of the cube. The nominal directions of the coordinate axes X_1, X_2, and X_3 are east, north, and up, respectively.

Inserting typical values for these quantities, namely $R = 1000$ m, $V_s = 1500$ m/s, and $d = 9.1$ m gives

$$\langle \Delta t^2 \rangle^{1/2} = 4.3 \times 10^{-6} \text{ (m/s)}^{-1} \langle \Delta x_i^2 \rangle^{1/2} \tag{5}$$

Spectral analysis of the position time series data shows the noise to be approximately white with a root-mean-square value of 0.2 m. This is close to the calculated value of the rms quantization noise resulting from digitization:

$$\langle \Delta x_q^2 \rangle^{1/2} = 1 \text{ count}/\sqrt{12} = 1 \text{ ft}/\sqrt{12} = .09 \text{ m} \tag{6}$$

Thus it can be concluded that timing jitter is still the primary source of noise in the data and that the rms value for the timing jitter ($\langle \Delta t^2 \rangle^{1/2}$) is 8×10^{-7} s.

Since this noise was the limiting factor affecting the accuracy of the present measurements, any improvements to the technique would have to be made by first reducing this source of noise. As can be seen from Eq. (4) the position uncertainty increases as the slant range increases. Thus, to apply this technique in the open ocean where the water depths are five times greater than those near St. Croix would require that either the timing jitter be reduced or the array dimensions be increased, or both. Since the present array dimension of 9 m is already large, any attempt to use a larger geometry would probably require that the rigid configuration be abandoned in favor of independently moored hydrophones. Increased accuracy of the timing measurement may also be possible; however, since the present timing uncertainty is already down to one fifteenth of one cycle of the 75 kHz "ping," this may prove to be difficult.

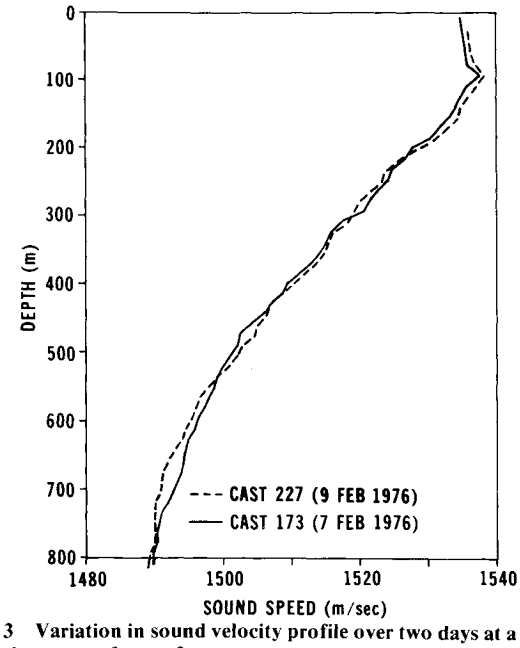

Fig. 3 Variation in sound velocity profile over two days at a location near the center of array 3.

Another source of error has to do with the uncertainty in the time when the acoustic pulse was emitted. Since the internal clock used to time this pulse will drift, there will be an error in the computed position, which grows with time. The error in the inferred velocity can by shown to be approximately

$$\Delta v_i \cong (x_i V_s D)/R \tag{7}$$

where V_s is the speed of sound, R is the slant range, and D is the clock drift rate in s/s. The clocks used for these measurements drifted at a rate of 10^{-7} s/s. Putting $x_i = 500$ m (typical maximum), $V_s = 1500$ m/s and $R = 500$ m gives a velocity error of 1.5×10^{-4} m/s.

Measurements of the sound velocity profile were made daily using a Plessey 9040 CTDSV (SV refers to a sound velocity sensor included in this profiler), and were updated in the tracking computer every several days. Figure 3 shows the amount of variability in the sound velocity profile over the several days between profile updates in the tracking computer. As can be seen from the figure, typical variations in the sound speed were on the order of 1 to 2 m/s. The variability over longer periods of time (up to 1 month) was also examined; it was not substantially greater, being approximately 2 to 3 m/s.

A schematic for the current profilers is shown in Fig. 4. The fins near the lower end were used to cause the profilers to revolve about once for each 3-m depth change, thereby removing any tendency they might have to lift in a particular lateral direction. To keep the profilers from tilting significantly during descent, items whose locations were arbitrary were positioned near the bottom end of the pressure vessel. This resulted in a buoyant restoring torque of approximately 2.7 Nm/deg of tilt. This value is large enough to guarantee that even maximum torques caused by current shear will produce deflections no greater than a very small fraction of a degree. To check for hydrodynamic instabilities, the profilers were tilted by divers during their descent. The resulting tilt oscillations had a period of approximately 2.0 s and were rapidly damped.

For most of the drops, the descent and ascent rates of the profilers were adjusted to approximately 0.3 m/s. The amounts of fixed and dropable ballast necessary to give this speed on both ascent and descent were determined from the measured drag coefficient [86 N/(m/s)^2]. Between the surface and 400 m (typical maximum depth), the buoyant force on the profilers would increase by about 2.2 N; therefore, at least this amount of initial net ballast was necessary to prevent stalling. By ballasting them to 8 N heavy on descent, the possibility of stalling was eliminated and unwanted variations in descent speed were kept below about 15%.

During some of the current profiler drops, the local profile of Väisälä frequency was measured with a Plessey 9040 CTDSV. The procedure that was followed was to position the CTD boat directly over the descending current profiler, and then to initiate the CTD cast as the profiler passed a depth of 250 m. Using the tracking information from the acoustic range, it was typically possible to start the CTD cast within 80 m of the point where the profiler was dropped. During the descending portion of the CTD cast, the boat would usually drift a total of 80 m, causing the average position of the CTD cast to be about 40 m from its start location. Thus, the average horizontal displacement between the CTD sensor and the current profiler was on the order of 100 m. The average time lag was about 10 min.

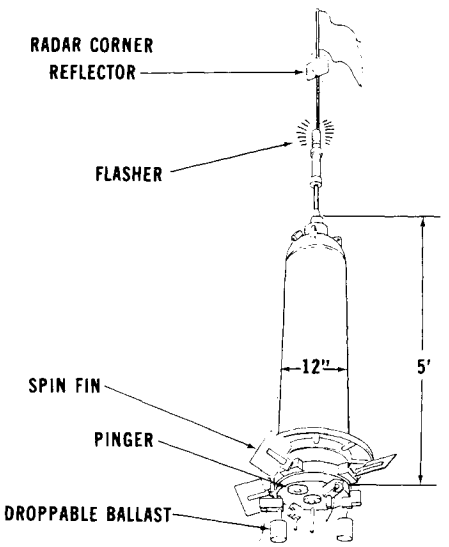

Fig. 4 Current profiler schematic. The instrument is released from the surface and descends until a pressure-actuated mechanism releases a pair of ballast weights. If the instrument stalls before releasing primary ballast, then a timed electrical weight release is fired. The electrical release is also activated by low battery voltage to allow recovery before acoustic tracking is lost.

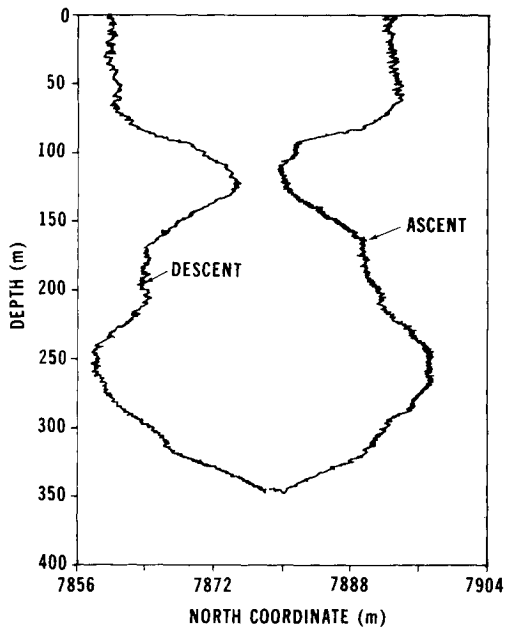

Fig. 5 North component of raw tracking data for drop 36J (Feb. 9, 1976).

Data Processing

Figure 5 shows a high-resolution plot of the profiler tracking data. The point-to-point noise in the data is due to timing jitter and also to quantization noise resulting from the fact that the positions were only recorded to the nearest integer number of ft.

To compute the profiler velocities, the x, y, and z position time series were first individually wild-point edited, the gaps were filled in by linear interpolation, and the velocities were then computed by taking the slope of a centered running quadratic least-squares fit to the data. A second pass with the quadratic filter was then used to compute the derivatives of both horizontal velocity components with respect to depth (shear), and at the same time to perform additional smoothing of the velocity data. It should be noted that this technique of least squares fitting a parabola to produce estimates of the function and its derivative at the center of the data interval is a linear process which produces no phase shifting in the pass band.

Figures 6 and 7 show typical profiles of velocity and shear obtained by this method. The agreement between the ascending and descending measurements gives an indication of the accuracy obtained. Near the bottom of the profile (where temporal variability is less important), the two measurements agree to about 0.5 cm/s in velocity and -10^{-3} m/s/m in shear.

To maintain a fixed bandpass in vertical wavenumber, the filter smoothing span was adjusted to a fixed depth interval by varying the number of points in the fit in inverse proportion to the profiler descent speed. The smoothing span that was used for all of the results presented in this article was 15 m. To calculate the wavenumber resolution present in the velocity

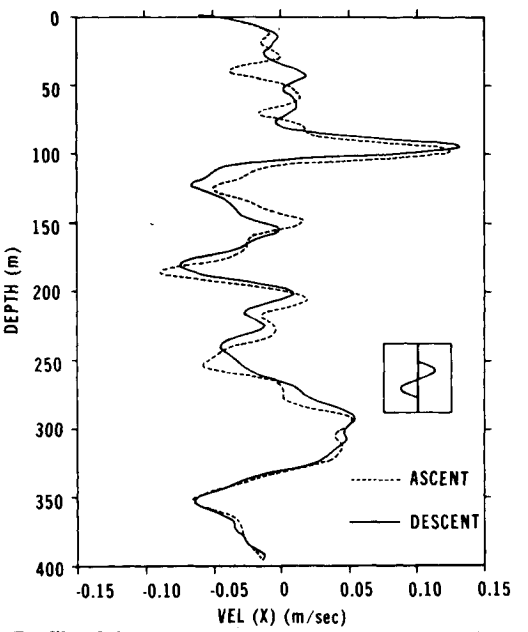

Fig. 6 Profile of the east component of current for drop 33 in array 3 (Feb. 9, 1976) obtained using a running quadratic least-squares fit to the position time series of the current profiler. The insert shows the shortest wavelength nominally passed by the quadratic filter.

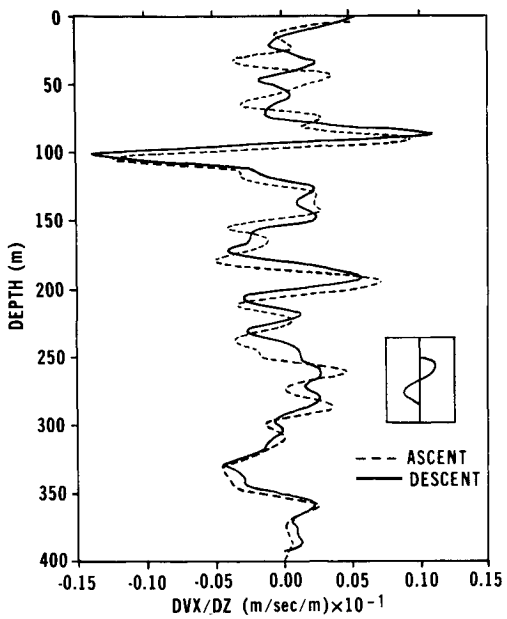

Fig. 7 Profile of the east component of shear for drop 33 (Feb. 9, 1976) computed using a running quadratic least-squares fit to the velocity profile shown in Fig. 6. The shortest wavelength nominally passed by the quadratic filter is shown in the insert.

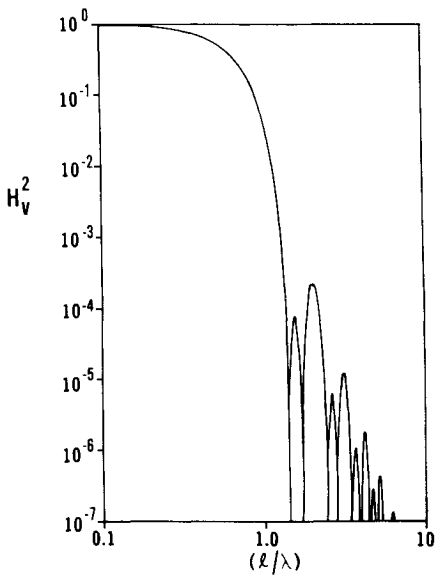

Fig. 8 Frequency response of filter used to compute velocity, plotted vs the filter smoothing span in wavelengths.

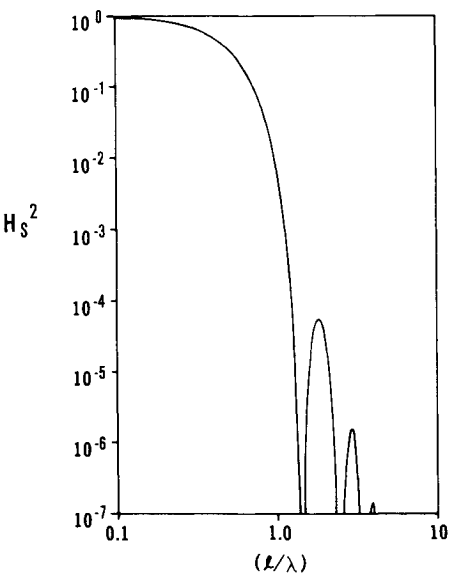

Fig. 9 Frequency response of filter used to compute current shear, plotted vs the smoothing span in wavelengths.

and shear profiles, it is necessary to consider the effects of applying the two quadratic filters in cascade. In the continuous approximation (i.e., infinite sampling frequency),‡ the response of the quadratic differentiator is given by

$$H_1 = \frac{3}{\beta^2}\left(\frac{\sin\beta}{\beta} - \cos\beta\right) \tag{8}$$

where H_1 is the ratio of estimated (smoothed) to actual (unsmoothed) velocity, and where

$$\beta = \pi(l/\lambda) \tag{9}$$

is a measure of the depth interval l spanned by the parabola relative to the wavelength λ of the input sinusoid. When the quadratic fit is used to smooth the data (by taking the value of the parabola at its midpoint as the smoothed value), then the response is given by

$$H_2 = \frac{3}{2\beta}\left[\left(\frac{5}{\beta^2} - 1\right)\sin\beta - \frac{5}{\beta}\cos\beta\right] \tag{10}$$

where H_2 is the ratio of the amplitude of the output sinusoid to the amplitude of the input sinusoid, and where β is as defined before.

Since the velocities were computed by quadratic differentiation followed by quadratic smoothing, the net frequency response is the product of the individual frequency response functions:

$$H_v = H_1 H_2 = \frac{9}{2\beta^3}\left(\frac{\sin\beta}{\beta} - \cos\beta\right) \times\left[\left(\frac{5}{\beta^2} - 1\right)\sin\beta - \frac{5}{\beta}\cos\beta\right] \tag{11}$$

‡The actual least-squares fit was done on approximately 40 points, which is a large enough number so that the assumption of continuous sampling only leads to several percent errors in the calculation of the frequency response function in the passband of frequencies. If the actual filter span (l) is replaced by $l(N/N-1)$, where N is the number of points used in the discrete case, then the continuous approximation for H_1 is accurate to within 0.1% in the passband for the case of a 41-point fit.

where H_v is the ratio of the final velocity estimate to the unsmoothed velocity. The square of this function is plotted in Fig. 8. This filter rolls off to half power at a wavelength λ of approximately 1.8 times the smoothing span. Similarly, the frequency response function for the vertical shear components ($s = dv/dz$) is given by

$$H_s = H_1^2 = \frac{9}{\beta^4}\left(\frac{\sin\beta}{\beta} - \cos\beta\right)^2 \tag{12}$$

The square of this function is plotted in Fig. 9. This response is similar to that for velocity, except that here the half-power point occurs at a value of the wavelength about 2.4 times the smoothing span. Since the filter span was always 15 m, the computed velocities have a nominal resolution of 27 m and the shears have a slightly lower resolution of 36 m.

It is clear from the graph of shear (and velocity to some extent) that there is significant energy near the filter cut-off, and therefore that some real small-scale fluctuations have been modified or eliminated by filtering. This effect was unavoidable, since reduction in the filter span below 15 m

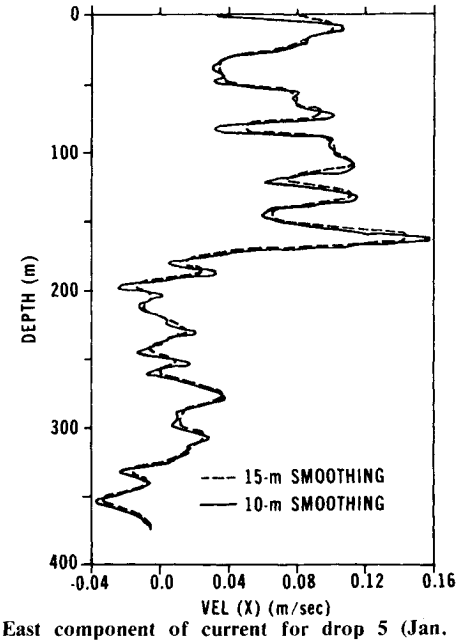

Fig. 10 East component of current for drop 5 (Jan. 22, 1976) calculated using filter-smoother spans of 10 and 15 m.

usually tended to pass more noise energy than signal and generally reduced the agreement between the up and down profiles. Occasionally however, the tracking data were good enough so that the filter span could be reduced. Figure 10 shows one case where it was possible to reduce the filter span to 10 m and still achieve very good agreement between the up and down profiles.

It would be interesting to compare the accuracy of the present measurements with that obtained by investigators working in the open ocean. Unfortunately, nearly simultaneous up-down profiles which could be used to assess accuracy of these other measurements do not appear to be available. Pochapsky,[6] who used a long-base-line transponder system, estimated that approximately 0.5 cm/s residual noise remained after filtering out scales less than 100 m. This is far§ less than the present measurements, where approximately the same level of noise was obtained but with approximately two octaves increased bandwidth in vertical wavenumber. Rossby,[5] using an existing hydrophone array in place near Bermuda, also filtered out scales less than 100 m but did not estimate the residual noise in this band.

More recently Sanford,[8] using an electromagnetic profiler, obtained velocity profiles with 10 m vertical resolution and an rms error of 1 cm/s. This performance is comparable or perhaps superior to that reported here; however, his technique only gives the velocity profile to within an unknown additive constant and hence cannot be used to measure absolute velocities.

Results

To gain an understanding of the nature of the spatial and temporal variability of the current field west of St. Croix, measurements were made in May 1975 and during January and February 1976. In all, 58 drops to a nominal depth of 400 m were made at various locations and times. To characterize the temporal variability of the currents and shears on the range, the profilers were dropped every several hours at a fixed location (near the center of array 3). In conjunction with these time-series measurements, information on the spatial variability of the current profile was obtained by dropping a

§Since the positional noise is approximately white, the noise velocity spectrum will be proportional to f^2; thus, the noise variance will be dominated by high frequencies. Filtering out the top two octaves will give a drastic (64×) reduction in velocity noise variance.

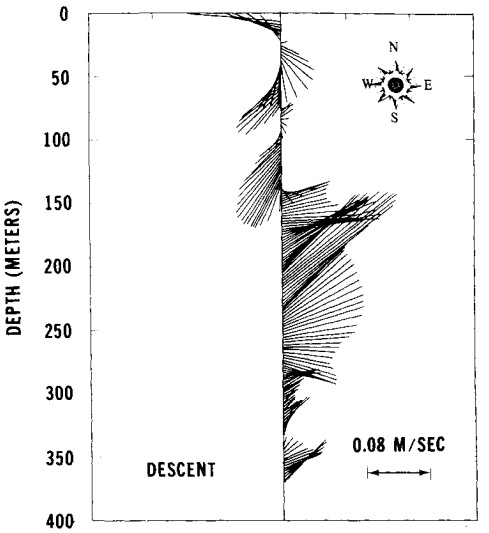

Fig. 11 Ocean current vectors plotted vs depth for current profiler drop 2 (May 19, 1975).

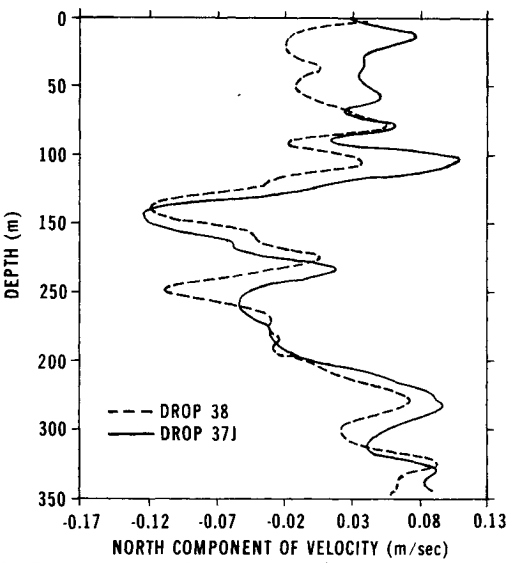

Fig. 12 Variation in north component of current over a time span of 2 h measured at a fixed location (near array 3 center).

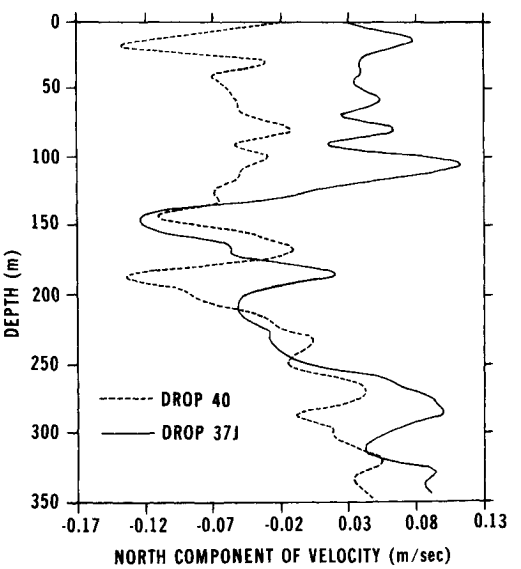

Fig. 13 Variation in the north component of velocity over a period of 4 h.

second profiler at different locations on the range at the same times that the first profiler was being dropped at the time-series locations.

All the profiles almost independently of time or position on the range showed a great deal of vertical variability in both the magnitude and direction of the current vector. Figure 11 shows a profile which more or less typifies all of those measured. As can be seen from the figure, the currents range in magnitude from 0 to about 20 cm/s and no particular direction seems to be clearly preferred. Also, reversals in direction and large changes in current magnitude typically occur over depth intervals on the order of 50 to 100 m.

Comparison of velocity profiles from time-series drops reveals a large amount of temporal variability, as well. This is shown in Fig. 12, where the north component of velocity is plotted versus depth for the two drops at the same location (near array 3 center) but separated in time by 2 h. The amount of variability shown is similar to that observed for other time-series drops that were separated by the same time interval. Over intervals of time much longer than this, the similarity evident in Fig. 12 was usually observed to be lost, as can be seen from Fig. 13, where the earlier of the two drops shown in Fig. 12 is plotted with a drop made 4 h later.

Since on the average, the 26 time-series drops (all near the center of array 3) were placed within 80 m of the target location, it is doubtful that this uncertainty could have accounted for the variations observed (see the discussion on spatial variability later in this section). It is possible, though, that advection of spatial inhomogeneities past the time-series location could have been the cause of part of the variability. However, since the average drift of the top 300 m of water was usually equivalent to 5 cm/s (which is much less than typical internal wave phase speeds), it is reasonable to believe that most of the measured temporal variability was real.

To gain additional information on temporal variability, a linear array of VACM's (vector averaging current meters) was implanted near the time-series location in array 3. Good records of currents and temperature were obtained at depths of 95, 144, 193, and 243 m for a period of 31 days, beginning February 20, 1976. No current-profiler drops were made during this period to allow direct comparison; however, the current magnitudes and variability measured appeared to be similar to those measured during the earlier periods with the profilers.

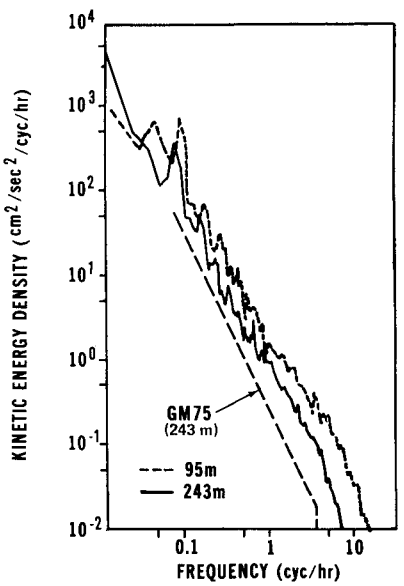

Fig. 14 Spectrum of the north component of velocity from current meter array deployed near the center of array 3. Record length was approximately 1 month beginning Feb. 20, 1976.

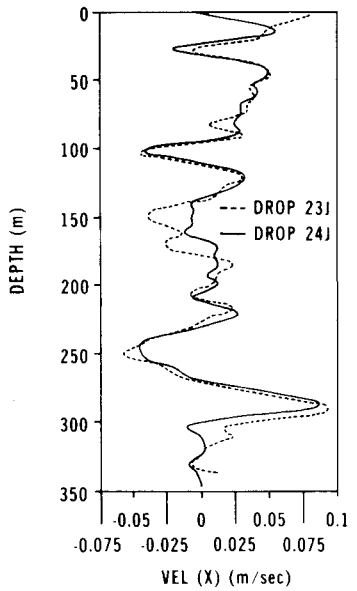

Fig. 15 Variation in the east component of current for two simultaneous drops separated by 500 m along a north-south line.

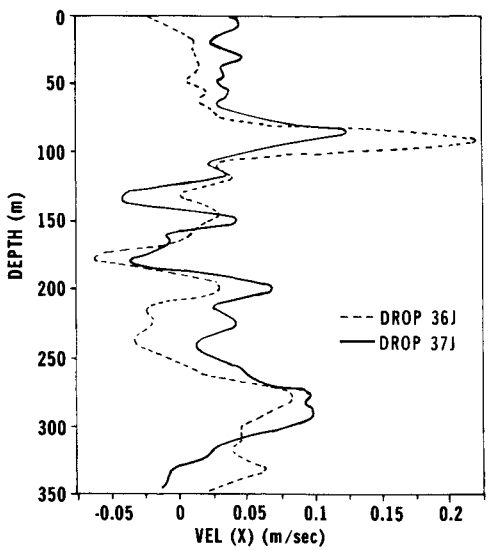

Fig. 16 Variation in the east component of current for two drops separated by 1.9 km along a north-south line.

Figure 14 shows the spectra that were computed from the current sensors located at 95 and 243 m. The spectra are quite similar in appearance, with the shallower record showing approximately twice the energy. This is consistent with the expected behavior for internal waves in the WKBJ approximation, since the Brunt-Väisälä frequencies at these depths were approximately in the same ratio (9:4 cph). Also consistent with expected internal wave behavior is the fact that both spectra show an abrupt decrease in slope at frequencies beyond the local Brunt-Väisälä frequency.

The dashed line in Fig. 14 shows the prediction of the supposedly universal spectral model of Garrett and Munk[2] for the current meter at 243 m depth. Near the frequency of 0.2 cph, where Wunsch[9] examined the geographical variability of the deep ocean internal wave field, it can be seen that the observed spectral density is approximately two times that predicted by Garrett and Munk. Thus, it would appear that the shallow water depth at St. Croix (1000 m) may be responsible for an increased level of internal wave activity. This factor-of-2 increase in energy was also exhibited for the 3 other current meters on the array at depths ranging from 95 to 190 m.

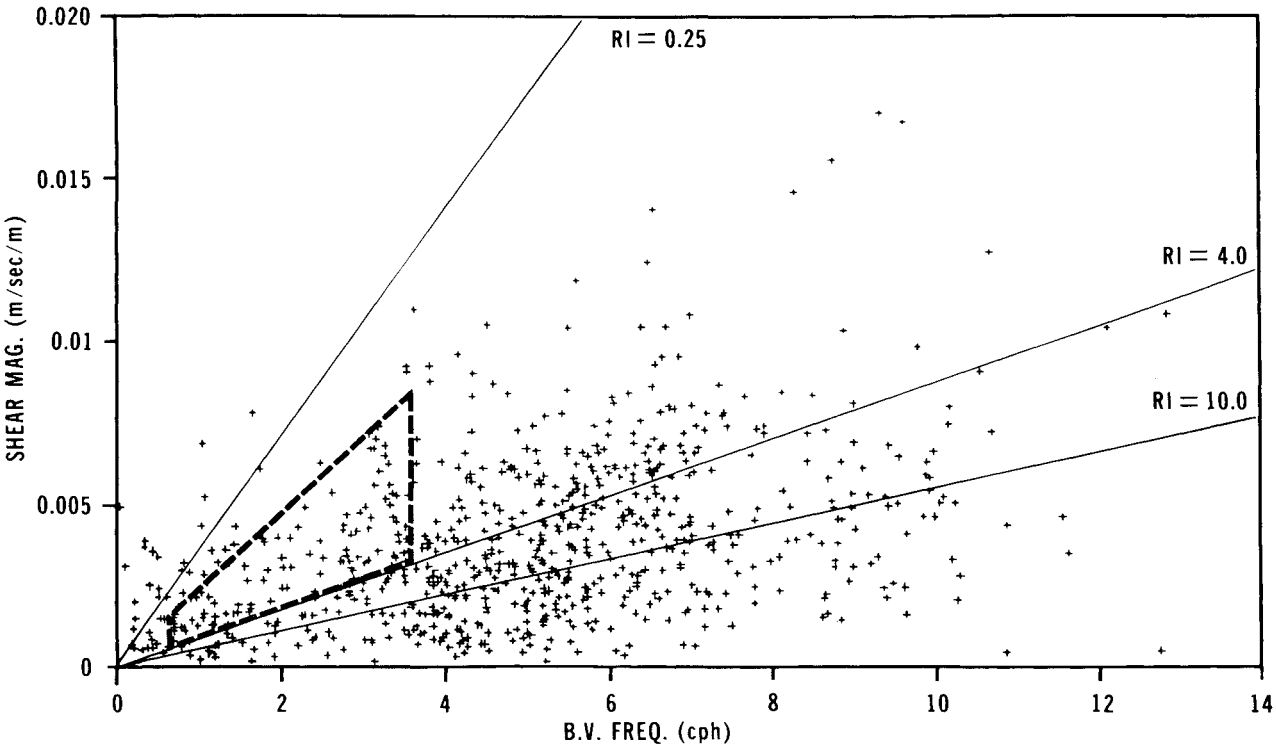

Fig. 17 Shear magnitude plotted vs Brunt-Väisälä frequency for six drops measured in January and February, 1976. The dashed lines enclose the area occupied by the majority of the Richardson numbers measured by Sanford[8] in the open ocean.

The measurements of spatial variability made by dropping two profilers simultaneously revealed a surprising degree of horizontal homogeneity of the current field. This can be seen in Figs. 15 and 16, which show the variation in the profile of the east component of current for joint drops separated along a north-south line by 0.5 and 1.9 km, respectively. The variability of the north (longitudinal) component of velocity appeared to be similar to that for the east (transverse) component, showing a coherence length on the order of several km; however, no statement can be made until a statistical analysis has been completed. This work is underway and will be reported at a later time.

The results for the profiler/CTD drops are summarized in Fig. 17, which shows shear magnitude plotted versus local Brunt-Väisälä frequency for six drops measured in mid-January and early February of 1976. The Brunt-Väisälä frequency (N) was computed from

$$N^2 = g^2\{(\partial\rho/\partial T)_{S,P}[(\mathrm{d}T/\mathrm{d}P) - \tau] + (\partial\rho/\partial S)_{T,P}(\mathrm{d}S/\mathrm{d}P)\} \tag{13}$$

where T and S are the temperature and salinity, and where τ is the adiabatic temperature gradient,

$$\tau = (\partial T/\partial P)_{\eta,S} \tag{14}$$

The adiabatic temperature gradient was computed according to Bryden,[10] and the density was computed using an empirical formula due to Ekman.[11] The computational procedure for N involved calculating the difference in density of two fluid elements after they had been transferred isentropically ($\Delta\eta = 0$, S = constant) to the mean pressure between the two levels considered. This procedure was modified to allow filtering of the gradient by transferring a group of points isentropically to the group's mean pressure and then calculating a density gradient by taking the slope of the quadratic least-squares best fit to the data. The filter span used was 15 m to give approximately the same bandpass as for the shear estimates.

As can be seen from Fig. 17, The Richardson number

$$R_i = N^2 \Big/ \left\{\left(\frac{\mathrm{d}u}{\mathrm{d}z}\right)^2 + \left(\frac{\mathrm{d}v}{\mathrm{d}z}\right)^2\right\} \tag{15}$$

seldom goes below the critical value of 0.25, indicating that probably no actual instabilities were measured. However, the fact that near-critical shears were encountered during a significant fraction of the time makes it seem probable that instabilities do occur intermittently, which then act to bring the Richardson numbers back above critical. Due to the inability of this technique to resolve the high-wavenumber portion of the current profile, it cannot be determined how frequently supercritical shears would be encountered in a fully resolved profile.

Also shown in Fig. 17 are the measurements of Sanford[8] taken in the open ocean during the Mid-Ocean Dynamics Experiment. Although a direct comparison cannot be made, due to the differences in depth and resolution of the measurements, it is clear that both results show similar high levels of shear bordering on instability.

Summary and Conclusions

To summarize, the results of this study tend to indicate that the internal waves were the dominant source of variability in the current field observed near the island of St. Croix. Measurements of gross (i.e., not fully resolved) Richardson number profiles showed few actual instabilities ($R_i \leq 0.25$), but the fact that a large number of Richardson numbers near unity were observed suggests that shear instabilities probably did occur periodically, serving to limit the amplitude of the internal wave field.

Acknowledgments

The engineering and deployment of the current meter array were done by the Woods Hole Oceanographic Institution under the direction of R. Walden. The current meter data were reduced by S. Tarbell and R. Payne,[12] also of the Woods Hole Oceanographic Institution. The assistance of T. Rossby

of the University of Rhode Island in certain aspects of the design of the current profiles is also gratefully acknowledged. The essentially perfect functioning and successful recovery of the current profilers through numerous deployments were due to the excellent mechanical engineering work done by R. A. Mattey of the Johns Hopkins University Applied Physics Laboratory.

References

[1] Garrett, C. J. R. and Munk, W. H., "Space-Time Scales of Internal Waves," *Geophysical Fluid Dynamics*, Vol. 2, 1972, pp. 225-264.

[2] Garrett, C. J. R. and Munk, W. H., "Space-Time Scales of Internal Waves: A Progress Report," *Journal of Geophysical Research*, Vol. 80, 1975, pp. 291-297.

[3] Desaubies, Y. J. F., "Analytical Representation of Internal Wave Spectra," *Journal of Physical Oceanography*, Vol. 6, November 1976, pp. 976-981.

[4] Wunsch, C., "Deep Ocean Internal Waves: What Do We Really Know?" *Journal of Geophysical Research*, Vol. 80, 1975, pp. 339-343.

[5] Rossby, T., "Studies of the Vertical Structure of Horizontal Currents Near Bermuda," *Journal of Geophysical Research*, Vol. 79, 1974, pp. 1781-1791.

[6] Pochapsky, T. E., "Vertical Structure of Currents and Deep Temperatures in the Western Sargasso Sea," *Journal of Physical Oceanography*, Vol. 6, 1976, pp. 45-56.

[7] Sandstrom, W. M., "Three-Dimensional Underwater Geometry and Survey Procedures," University of Washington, Applied Physics Laboratory Tech. Manual 6917, Aug. 1969.

[8] Sanford, T. B., "Observations of the Vertical Structure of Internal Waves," *Journal of Geophysical Research*, Vol. 80, 1975, pp. 3861-3871.

[9] Wunsch, C., "Geographical Variability of the Internal Wave Field: A Search for Sources and Sinks," *Journal of Physical Oceanography*, Vol. 6, 1976, pp. 471-485.

[10] Bryden, H. L., "New Polynomials for Thermal Expansion, Adiabatic Temperature Gradient, and Potential Temperature of Sea Water," *Deep-Sea Research*, Vol. 20, 1973, pp. 401-408.

[11] Fofonoff, N. P., "Physical Properties of Sea-Water," *The Sea*, Vol. 1, M. N. Hill, ed., Interscience Publishers, New York, 1962, p. 11.

[12] Tarbell, S., Payne, R., and Walden, R., "A Compilation of Moored Current Meter Data and Associated Mooring Action Data from Mooring 592," Vol. XIV (1976 Data), Woods Hole Oceanographic Institution Rept. 77-41, Sept. 1977.